REPORT DOCUMENTATION PAGE

Form Approved OMB No. 0704-0188

1. AGENCY USE ONLY (Leave blank)	2. REPORT DATE	3. REPORT TYPE AND DATES COVERED
	March 1997	Final Report

4. TITLE AND SUBTITLE

Wind Tunnel Wall Effects on the Flow around a 76/40-deg Double-Delta Wing

5. FUNDING NUMBERS

F6170896W0094

6. AUTHOR(S)

Prof. Nicolaas Goris Verhaagen

7. PERFORMING ORGANIZATION NAME(S) AND ADDRESS(ES)

Delf University of Technology
Dept. of Aerospace Engineering
P.O. Box 5058
Delft 2600 GB
Netherlands

8. PERFORMING ORGANIZATION REPORT NUMBER

N/A

9. SPONSORING/MONITORING AGENCY NAME(S) AND ADDRESS(ES)

EOARD
PSC 802 BOX 14
FPO 09499-0200

10. SPONSORING/MONITORING AGENCY REPORT NUMBER

SPC 96-4008

11. SUPPLEMENTARY NOTES

12a. DISTRIBUTION/AVAILABILITY STATEMENT

Approved for public release; distribution is unlimited.

12b. DISTRIBUTION CODE

A

13. ABSTRACT (Maximum 200 words)

This report results from a contract tasking Delf University of Technology as follows: The contractor will perform a service consisting of experimental investigations of the effect of small geometry modifications at the strake/wing junction of a cropped double delta wing. The investigations will include the effect of ts on surface pressure, forces, and moments for an existing double delta wing wind tunnel model at NAWC. Testing will take place in the NAWC low-speed wind tunnel facility and the experimental data will be compared with existing dat m NASA Langley and compared with new CFD predictions described in his proposal.

14. SUBJECT TERMS

Aircraft Subsystem, Control System

15. NUMBER OF PAGES

38

16. PRICE CODE

N/A

17. SECURITY CLASSIFICATION OF REPORT	18. SECURITY CLASSIFICATION OF THIS PAGE	19. SECURITY CLASSIFICATION OF ABSTRACT	20. LIMITATION OF ABSTRACT
UNCLASSIFIED	UNCLASSIFIED	UNCLASSIFIED	UL

March 1997

Re: EOARD Special Contract Program SPC 96-4008

Wind Tunnel Wall Effects on the Flow around a 76/40-deg Double-Delta Wing

by

N.G. Verhaagen
Delft University of Technology (TUDelft)
Department of Aerospace Engineering
P.O. Box 5058, 2600 GB Delft
the Netherlands

Abstract

Surface-pressure data of a 76/40-deg double-delta wing tested in the BART wind tunnel at NASA LaRC have been corrected for tunnel wall and support interference effects. The correction is shown to improve the correlation between the computed and measured pressure data. Overviews are given of existing tunnel wall correction procedures for wings with leading-edge vortex separation and of studies that investigate the effect of tunnel walls on the vortex burst location.

Contents

1 Nomenclature

B	tunnel span
b	wing span
c	root chord length, = 2.406 m (16 in.)
$\bar{c}$	mean aerodynamic chord
C_D	drag coefficient
C_{D_S}	separation drag coefficient
C_L	lift coefficient
C_N	normal force coefficient
C_p	static pressure coefficient, $= (p - p_\infty)/q_\infty$
C_{pt}	total pressure coefficient, $= (p_t - p_\infty)/q_\infty$
H	tunnel height
M	freestream Mach number
p	static pressure
p_t	total pressure
p_∞	freestream static pressure
q_∞	freestream dynamic pressure
R_b	b/B
R_t	H/B
Re	Reynolds number, based on root chord length
s	local wing semispan
x, y, z	coordinates of wing axes system, origin at apex
α, AOA	angle of attack
Λ	leading-edge sweep angle

2 Introduction

Modern NAVY fighter aircraft are designed to rely on the enhanced lift generated by vortex flow to enable high maneuverability. Vortical flows are part of the overall flow structure of these aircraft. Current designs result in the shedding of vortices from various locations on the aircraft including the forebody, moderate to highly swept wing leading edges, strakes and leading edge extensions, and the junction of aerodynamic surfaces with each other and the fuselage. The shedding, interaction and breakdown of these vortices are highly sensitive to both the aircraft geometry and the flow conditions. In addition to producing the benefits of enhanced lift and maneuverability, the vortical flow also causes serious departure and structural fatigue problems, e.g., the vortex tail buffet phenomenon of F/A-18 aircraft. Techniques for controlling the trajectory, strength and breakdown processes of the vortices may not only alleviate the problems generated by this flow phenomenon, but also enhance the existing controllability, maneuverability and agility of the aircraft.

In a numerical study, Kern [1] of NAWC (Naval Air Warfare Center) investigated the effects of small deployable fillets at the junction of the strake/wing leading edge of a cropped double-delta wing. The strake and wing leading edges had a sweep angle of 76 and 40 deg, respectively, forming a baseline planform representative of highly-maneuverable aircraft. The fillets investigated had a linear, parabolic and diamond shape. The numerical predictions indicated that the fillets do affect the shedding process at the junction of the strake/wing leading edge and thus the trajectories, vortex interaction and breakdown of the vortices over the double-delta wing. At an angle of attack of 10 deg., which is in the range of Naval aircraft approaching a carrier for landing, the fillets were predicted to shift the vortex structure outboard. This potential may lead to a method of alleviating tail buffet by deflecting the vortices away from the tail surfaces. Through asymmetric deployment of the fillets, additional lateral-directional control may be realized. At an angle of attack of 22.5 deg, which is the angle of attack at which Naval aircraft maneuver, the fillets delayed vortex breakdown by providing a favorable vortex interaction. The delay in breakdown enhances the lift with a slight improvement in lift-to-drag ratio.

For a validation of the numerical predictions, experimental tests are necessary to generate data on the effect of fillets on the vortex flowfield, induced wing surface pressures and forces and moments at various angles of attack and sideslip. To obtain this data, NAWC constructed a 76/40-deg double-delta wing model (Fig. 1). In the frame of a cooperative research effort between the NASA LaRC (Langley Research Center) and NAWC, this wing was tested at different test conditions in the LaRC 8-ft tunnel, the 7-ft by 10-ft tunnel and the BART (Basic Aerodynamic Research Tunnel).

The testings in BART were carried out on the baseline configuration of the double-delta wing (so without fillets) and included flow visualization tests, surface pressure recordings and flowfield surveys. The data were used to validate solutions of the thin-layer Navier-Stokes equations for fully laminar flow obtained by Kern. The study, reported by Verhaagen, et al, [2] showed the solutions to well predict the behavior of the flow on and off the upper surface of the baseline double-delta wing. However, large differences were found between the predicted and measured upper-surface pressure distributions. These

differences were due to the fact that the tunnel wall and model support interference effects were not fully taken into account, both in the testings and the predictions.

Interference of the tunnel walls and model support results into an increase in dynamic pressure of the flow around the wing due to solid and wake blockage. In addition, lift interference and streamline curvature effects change the angle of attack.

The objective of the study described in the present report was to apply wall and support interference corrections to the test data and to compare the corrected data with the numerical solutions. In addition, to discuss published data on the effect of tunnel walls on the breakdown of leading-edge vortex cores. A summary of the BART test setup and results is given in section 3. An overview of existing wall interference correction methods is given in section 4, while the effect of the corrections on the test data and on the comparison with the solutions is discussed in section 5. Finally, the effect of tunnel walls on the vortex core breakdown location is discussed in section 6.

The present study has been conducted in the frame of EOARD Special Contract Program SPC 96-4008.

3 BART Experiment

3.1 Wind Tunnel

The tests were carried out in the BART of the NASA LaRC. This is a subsonic, open-return wind tunnel with a test section 0.71 m high, 1.02 m wide and 3.05 m long (Fig. 2). The variation in longitudinal turbulence intensity ranges from approximately 0.03% at an air speed of 15 m/sec to 0.09% at an air speed of 48 m/sec. Further details of the wind tunnel facility can be found in reference [3] by Sellers and Kjelgaard.

3.2 Model

The model was a stainless steel 76/40-deg swept double-delta wing designed and provided by NAWC (Fig. 1). The model had a chord length of 0.406 m (16 inches), a span of 0.415 m and thickness of 9.53 mm. The leading-edge kink was situated at 52% chord and the wing tip was cropped from the 84% chordwise station. The sharp leading and trailing edges of the model were broken and rounded to a diameter of 0.13 mm (0.005 in.). The under surface was beveled at 20 deg over a width of 26.16 mm. The kink section was capable of allowing fillets of different leading edge geometry to be installed. In the BART only the baseline configuration with straight strake and wing leading edges was tested. The left upper surface of the model was equipped with 48 pressure orifices of 0.25 mm (0.010 in.) diameter. Ten orifices were drilled in a spanwise row at 25% chord, while 19 orifices were drilled both at 75% and 90% chord. The pressure tubes exited the model at its lower surface. The model was supported in the tunnel by an internal-balance sting attached to its lower surface (Fig. 3). A fairing was fitted to the lower surface of the model to cover the balance block and the pressure tubes. The angle of attack of the model was set with a remotely controlled sting/post support. The angle of attack was monitored with an accelerometer mounted on the sting at a short distance behind the trailing edge of the model. The maximum uncertainty in the angle of attack reading was 0.03 deg.

3.3 Experimental Tests

A smoke/laserlight-sheet technique was used to visualize the structure of the vortex flow and to study probe/vortex interference effects. A single column of vaporized propylene glycol was introduced upstream of the tunnel inlet and positioned such that it could be entrained into the vortices generated by the model. A 6-Watt Argon-ion laser and a twin-mirrored galvanometer laserlight-sheet generator were used to illuminate the propylene glycol particles and thus the vortices. Two cameras were set at different viewing angles to capture the flow in planes both normal and parallel to the surface of the model. The laserlight-sheet technique was used at angles of attack ranging from 5 to 22.5 deg and a Reynolds number (Re) of mostly 0.5 million (M).

Surface flow visualization was used to determine the location of stagnation, attachment and separation lines in the boundary layer pattern on the upper surface of the model. This pattern was visualized using a mixture of titanium dioxide (TiO2) and kerosene.

The surface flow pattern was investigated at angles of attack ranging from -10 to 22.5 deg and Re = 0.5, 1.0 and 1.5 M.

The distribution of the upper-surface Cp at the 25, 75 and 90% chordwise stations was measured at angles of attack ranging from -5.0 to 25.0 deg and Re = 1.0 M. To study the effect of the Reynolds number on Cp, at α = 10 and 22.5 deg pressures were acquired at Re ranging from 0.5 to 1.5 M. While preparing the model for the surface pressure measurements, 2 of the 10 pressure ports at 25% chord were found to be unreliable. Therefore, these ports were not used during the testings. The remaining 46 pressure ports in the model were connected to transducers with a maximum range of +/-1.0 p.s.i. and an uncertainty of 0.2%. The uncertainty in Cp is a function of the surface pressure and the dynamic pressure. For Re = 0.5, 1.0 and 1.5 M, the maximum absolute uncertainty in the measured Cp was estimated to be +/- 0.275, 0.079 and 0.031, respectively.

3.4 Test Results

Selected test data will be discussed in this subsection. Much more data can be found in the original test data reports [2].

Fig. 4 shows a picture of the strake and wing vortices at α = 10 deg illuminated by a laserlight sheet orientated such that it passed through the vortex axes. From the picture it is evident that the strake and wing vortices hardly interact at this angle of attack. Fig. 5 gives a planview of the vortex axes trajectories and core bursting locations observed at the various angles of attack. The interaction between the strake and wing vortices increases with the angle of attack due to the vortices increasing in size and strength. It can be noted that the vortices burst before they cross over.

Fig. 6 shows a picture of the boundary layer flow pattern at α = 10 deg and Re = 1.0 M. The characteristic features of the surface flow pattern are indicated in the sketch. The boundary layer flow pattern on the strake is characterized by outflow markings induced by the strake vortices and clear secondary separation lines. The attachment lines of the primary vortex flow is outboard of the symmetry plane. The secondary separation lines are straight, giving evidence of an approximately conical strake vortex flow. The boundary layer underneath the strake vortex separates at a spanwise position $y/s \approx 0.70$, indicating that the boundary layer is laminar. In the case of a turbulent boundary layer, separation would occur more outboard at $y/s \approx 0.85$ [4]. The topology of the crossflow over the strake is shown in the left sketch of Fig. 7. The free shear layer of the secondary vortex attaches just inboard of the leading edge and induces an inward directed flow on the surface (see insert sketch). This flow separates again at the tertiary separation line. Between the latter line and the secondary separation line a region of accumulated surface oil was visible in the experiment. The pattern showed markings of an outflow that is assumed to be induced by the tertiary vortex. The tertiary separation line was visible from near the apex to the leading edge kink. Downstream of the leading edge kink, this line disappears as the tertiary vortex is supposed to be entrained into the stronger wing vortex.

Downstream of the leading edge kink, at $\alpha = 10$ deg the shear flow pattern induced by the strake and wing vortices and accompanying secondary separation lines remain individually distinguishable up to the trailing edge. The conjectured topology of the crossflow at $\alpha = 10$ deg is shown in the right sketch of Fig. 7. It is characterized by a double-branched wing vortex core fed by vorticity from free shear layers that are connected to the wing leading edge and the strake vortex core.

As far as the effect of Reynolds number is concerned, on the strake the pattern changed little when Re increases from 0.5 to 1.5 M. There were no signs of boundary layer transition from laminar to turbulent. On the wing, the strake vortex secondary separation lines were clearly visible when $Re = 0.5$ and 1.0 M. From about the 65 % chordwise position, the secondary separation lines at $Re = 1.0$ M are located outboard those at $Re = 0.5$ M.

Fig. 8 shows the effect of the angle of attack on the upper surface Cp at 25% chord for $Re = 1.0$ M. The Cp-distribution has been plotted versus the wing lateral coordinate y, non-dimensionalized by the local wing semispan s. At $\alpha = 0$ deg, a small suction peak is induced by the weak strake vortex near the leading edge. Inboard of the suction peak, flow incident to the wing causes a region of positive Cp. The angle of attack has little effect on the crossflow structure sketched in Fig. 7. The size and circulation of the strake vortex, however, increases with the angle of attack, resulting in a growing suction peak. Outboard of this peak, the pressure curves rise slightly due to the influence of the secondary and tertiary vortices. The level of suction induced by these vortices is about the same as that induced by the primary vortex, confirming that the boundary layer underneath this vortex is laminar. In the case of a turbulent boundary layer, the suction induced by the primary vortex would be larger, while the opposite would be the case for the suction induced by the secondary vortex. There would probably be no tertiary vortex [5].

The effect of the angle of attack on the Cp-distribution at 75% chord, shown in Fig. 9, can be explained using Fig. 10, which illustrates the effect of the angle of attack on the topology of the crossflow at this station. The latter figure is based on the results of the flow visualization tests. At $\alpha = 0$ deg, a weak strake vortex suction peak and stronger wing vortex suction peak can be detected in the Cp-distribution. As the angle of attack is increased to 5 deg, a slight increase can be noted in the strake vortex suction peak and a strong increase of the suction induced by the wing vortices. Outboard of both the strake and the wing vortex suction peak, a suction peak is induced by the accompanying secondary vortex. Up to $\alpha = 5$ deg, the strake and wing vortices are small and not connected to each other. In the gap between these vortices flow is incident to the wing, causing a small region of positive Cp at about $y/s \approx 0.6$. When the angle of attack is increased further, the strake and wing vortex cores become interconnected. Up to $\alpha = 12.5$ deg, the suction induced by the strake and wing primary and secondary vortices can be seen to increase. The increase in suction of the wing vortex secondary vortex is only small. This may be due to the transition of the boundary layer underneath the wing vortex from laminar to turbulent which reduces the influence of the secondary vortex. Beyond $\alpha = 10$ deg, the strake and wing vortices start to coil around each other. The strake vortex moves closer to the wing surface and more outboard, while the wing vortex moves upwards and inboard. The effect of these displacements is noticable in the Cp-curves; up

to $\alpha = 20$ deg the suction peak of the strake vortex moves outboard and increases in size, while the suction peak of the wing vortex moves inboard and reduces rapidly. At $\alpha = 20$ deg, the wing vortex is overhead the strake vortex and only one suction peak is induced on each wing half. At $\alpha = 25$ deg, the pressure distribution is affected by the burst of the strake vortex core. As a result, the suction peak not only collapses, but also spreads in the spanwise direction. The latter is caused by the radial expansion of the burst vortex core, through which the circulation previously contained in a narrow core is redistributed over a wider region.

The effect of the Reynolds number on the Cp-distribution at $\alpha = 10$ deg was investigated by acquiring data at Re ranging from 0.5 to 1.5 M. At 25% chord, the effect of Re on the Cp-distribution is of the order of the measurement accuracy. At 75% chord, there is a clear effect in the region dominated by the strake vortex (Fig. 11). Due to the transition of the boundary layer underneath the strake vortex from laminar to turbulent, the secondary vortex and its suction have become nil at $Re = 1.5$ M. This is in accordance with the surface flow pattern where the secondary separation lines have vanished at this Re. As a result, the primary vortex is located closer to the wing surface, inducing a higher suction than at $Re = 0.5$ M. On the wing vortex side, transition of the boundary layer results in a smaller and more outboard located secondary vortex. As a consequence, the primary wing vortex is expected to move slightly outboard as well, explaining the slight outboard shift of the wing vortex suction peak that can be noted when Re is increased from 0.5 to 1.5M.

4 Wind Tunnel Wall Corrections

4.1 Tunnel Wall Effects

When a wing is tested in a wind tunnel the presence of the tunnel walls will affect the flow around the wing. As a result of blockage, buoyancy and lift interference the flow will be different from that around the wing in free air. The blockage is due to the presence of the wing, its supports and wake, and results in an increase of the dynamic pressure of the flow around the wing. Buoyancy is a result of the axial static-pressure variation in the tunnel test section. The lift interference is associated with the circulation around the wing and affects its angle of attack.

4.2 Overview of Wall Correction Methods

In this section an overview is given of the development of wall correction procedures for wings with leading-edge separation. It should be remarked that this is not an overview of all existing wall correction methods for this type of wings.

The first tunnel wall interference correction methods were developed in a time of limited computational capability and are generally referred to as the classical wall correction methods. One such method is the method developed by Garner and Rogers [6]. They model the wing by a lifting line and the wake by trailing vortices which are assumed to remain in the plane of the wing. The latter limits the application of the method to low angles of attack.

Frink [7] uses a free-vortex-sheet (FVS) theory and calculates an improved lift-interference correction for the angle of attack by taking into account the effect of the bending of the trailing vortices into the direction of the freestream.

To account for wake blockage effects, Maskell [8] developed a method based on the measured drag coefficient. This method was improved by Pass [9] for application to models with high blockage ratios. Many blockage correction methods assume that the pressure distribution over the wing is not affected by the wall confinement, or in other words, that the flow transition and separation location remains the same. This socalled principle of invariance under constraint may hold for sharp-edged (double-)delta wings but to lesser extent for large models of complete aircraft configurations. According to Pass [9], the principle of invariance under constraint may be considered valid for configurations with blockage ratios up to 15% (the 76/40-deg double-delta wing considered in this report has a blockage ratio of 10%).

A method for correcting the high-α aerodynamic characteristics of fighter aircraft configurations is the wall-pressure signature method developed by Hackett, et al [10]. This method has the advantage that changes in separation position on the model and wake geometry are automatically accounted for. A minus point is that wall pressures need to be recorded in an extended number of locations not only on the walls of the test section, but often also at locations upstream and downstream of the test section.

To avoid the limitations of the previous procedures, methods are currently developed that are based on CFD solutions for the flow around a model in a wind tunnel. Examples can be found in papers by Thomas and Lan [11], and Verhaagen, et al [12].

The abovementioned methods are discussed in greater detail in the following subsection.

4.3 Details of Wall Correction Methods

4.3.1 Method of Garner and Rogers

The method is based on linear potential flow theory and uses images to predict wall interference. The wing is modeled by a lifting line and its wake by trailing vortices which are assumed to remain in the plane of the wing.

The blockage of the flow in the tunnel due to the presence of the wing and its wake is assumed to increase the velocity around the model by an increment ΔU_B. The blockage factor ϵ_B, being the sum of the solid, wake and streamwise-velocity interference blockage factors ϵ_s, ϵ_w and ϵ_v, can then be written as

$$\epsilon_B = \epsilon_s + \epsilon_w + \epsilon_v = \frac{\Delta U_B}{U} \tag{1}$$

For a "small" three-dimensional wing (wing span less than 0.5 tunnel width) in a rectangular test section the solid blockage factor is given by ([6], equation 5.29)

$$\epsilon_s = \frac{TV}{C^{3/2}\beta^3}\left[1 + 1.2\beta\frac{t}{c}\right], \tag{2}$$

where

$$T = 0.65\sqrt{\frac{B}{H}} \tag{3}$$

and

B = tunnel width
H = tunnel height
V = volume of the wing
C = tunnel cross-sectional area
β = $\sqrt{1 - M^2}$
t = model thickness
c = root chord length

The wake blockage factor is given by ([6], equation 5.53)

$$\epsilon_w = \frac{1}{4}\frac{S}{C}\frac{C_D}{\beta^2} \tag{4}$$

If the wing is displaced vertically off the center of the tunnel, there exist both streamwise and upward interference velocities. The streamwise velocity perturbation creates another blockage effect, called the stream-velocity interference factor. This is expressed as ([6], equation 3.27)

$$\epsilon_v = \delta(\frac{d}{H}, \frac{B}{H})\frac{S.C_L}{\beta BH}, \tag{5}$$

where d denotes the distance from the wing to the tunnel floor.

In incompressible flow the blockage factor is applied directly to the dynamic pressure by

$$q = q_m(1+\epsilon_B)^2 \approx q_m(1+2.\epsilon_B), \tag{6}$$

where q_m is the measured dynamic pressure.

The lift effect is due to the lift interference and streamline curvature effects. These effects induce an upwash normal to the freestream which increases the effective α of the wing. The correction in velocity direction is averaged over the wing so that it can be applied to the angle of attack α.

Representing the wing by a semi-infinite vortex pair and using the image method to satisfy the boundary condition on the walls, the following correction is derived ([6], equation 3.182)

$$\Delta\alpha = \frac{SC_L}{C}\left[\delta_0 + \frac{c - x_p}{\beta H}\delta_1\right], \tag{7}$$

where

δ_0 = the averaged upwash interference parameter at the lifting line (0.25 $\bar{c}$)
δ_1 = the upwash interference due to streamline curvature
x_p = center of pressure

The parameter δ_0 ([6], equation 1.34) is a function of the wing-to-tunnel span ration R_b and the tunnel cross-section ratio R_t. The lifting line model assumes the trailing vortices to be in the plane of the wing. This implies that the corrections are in fact applicable for small angles of attack only.

Karou [13] applied the above corrections for blockage and lift effects to the balance data of a 76-deg delta wing tested in a tunnel with different R_t ratios at TUDelft. The data were recorded at angles of attack up to 22.5 deg. That is far below the angle at which vortex burst occurs over the wing ($\approx$ 35 deg). The corrected data for the three values of R_t collapsed to a single line which was shown to be in very good agreement with other experimental data.

4.3.2 Method of Frink

Frink [7] extended the lifting-line interference correction using a free-vortex-sheet (FVS) theory. By using the doublet distribution from the tunnel walls, which contains the pressure distribution induced by the delta wing, he computed upflow variations at the wing such as the streamline curvature and aerodynamic twist. Fig. 12 shows the effect of R_b on the streamline curvature predicted at the rootchord of a 65-deg swept delta wing for α = 15 and 30 deg. The upflow angle can be seen to increase with R_b and

along the rootchord with the angle of attack. Fig. 13 shows a similar tendency for the spanwise variation of the wall-induced aerodynamic twist. Using his FVS solution he further showed that the averaged upflow parameter δ_0 not only is a function of R_b and R_t, such as is assumed in the lifting-line theory of reference [6], but also depends on the angle of attack. In the lifting-line theory the trailing vortices are assumed to remain in the plane of the wing, limiting its application to angles of attack up to approximately 20 deg. Frink showed that if the bending of the wake vortices into the direction of the free stream is taken into account, δ_0 becomes a function of C_N and cosα, rather than C_L, and can be written as

$$\delta_0 = (\frac{\Delta\alpha}{C_N})(\frac{4R_t}{R_b^2.tan\Lambda}).cos^{p-1}\alpha \tag{8}$$

where the cosine power p will be near 1 if the angle of attack is small, and near 2 at larger angles. His solution does not provide a correction for blockage or streamline curvature. Frink computed corrections for a 65-deg delta wing tested in the NASA LaRC LTPT (Low-Turbulence Pressure Tunnel) and for a large ($R_b = 0.584$) semispan 76-deg delta wing tested in the TUDelft LTT (Low-Turbulence Tunnel) [12]. The corrections to the 65-deg delta wing flowfield were shown to be good for R_b values up to 0.5 and angles of attack up to 30 deg. For the 76-deg delta wing the effect of the averaged upflow angle appeared to be corrected satisfactory. The effects of streamline curvature were noted to be large, but no values were given.

4.3.3 Wake Blockage Correction Method

The correction method of Pass [9] was developed for semispan wings which are tested in small subsonic wind tunnels. The method is based on a model of bluff body flow proposed by Maskell [8]. Assuming an axi-symmetric wake, he derives the following relation for the change in dynamic pressure:

$$\frac{\Delta q}{q} = \frac{1}{k^2 - 1}.C_{D_S}.\frac{S}{C} \tag{9}$$

where k is the base pressure parameter and C_{D_S} the separation drag coefficient. He further assumed that the separation location of the body and wake flow is not affected by the wall confinement. His model is considered valid for (full) configurations with blockage ratios of up to 10%. The C_{D_S} can be determined from the C_L^2 vs C_D curve (fig. 14). This procedure works well for straight wings, but becomes problematic if the curve is non-linear such as in the case of (double-)delta wings. To make Maskell's correction procedure applicable to a wider range of semispan geometries, Pass conducted an extensive series of experimental tests on straight, tapered and delta wing configurations. Based on the test results an empirical alteration to Maskell's expression (equation 9) was developed specifically for semispan models with a blockage ratios up to 29%.

4.3.4 Pressure Signature Method

The wall pressure signature method of Hackett, et al, [10] makes use of the static pressure distribution measured along the tunnel walls. The socalled "interference" flowfield at the location of the wing is computed by using a (vortex or doublet) singularity distribution with a strength determined by the measured wall pressure distribution. Hackett, et al, suggest to measure pressures along the centerlines of the tunnel floor, ceiling and side walls. The method has the advantage that changes in separation position on the model and wake geometry are automatically accounted for. A minus point is that wall pressures need to be recorded in an extended number of locations on the walls of the test section. To verify the asymptotic behavior of the pressure distribution along the walls, it is often necessary to also take pressures at locations upstream and far downstream of the test section. The wall pressure signature method is reported to be applicable to aircraft geometries of blockage ratios up to 20% [9]. Care should be taken when applying this procedure to configurations with extended flow separation, such as present over delta wings at large angle of attack or sideslip. To determine the local singularities in the wall pressure distribution induced by the wing, its support and wake, it may be necessary to take pressures not only at the centerline of the tunnel walls but also at other wall locations.

4.3.5 Numerical Simulations

Thomas and Lan [11] used a thin-layer Navier Stokes solver to simulate the flow about a 76-deg delta wing in the BART at NASA LaRC. The tunnel wall pressures were not measured as in the former method, but were computed and used as the boundary condition for an Euler solution of the wind tunnel flow without the presence of the delta wing (Fig. 16). The computed interference flowfield was used to estimate the blockage and upwash effects needed to correct the wing forces to free air conditions. The corrected $C_L - \alpha$ curve was shown to agree well with the balance data obtained in the larger 7-ft by 10-ft (2.1-m by 3.0-m) wind tunnel at NASA LaRC.
Verhaagen, et al, [12] compute the flow over a large-size semispan 76-deg delta wing in the LTT of TUDelft using an Euler solver. The effect of R_b on the leading-edge vortex flow and the aerodynamic forces was determined from solutions developed for the flow around the wing in tunnels of different cross-sectional geometries and for the wing in free air. The solutions showed that an increase of R_b results into an increase of the magnitude of the velocities and pressures in the vortex core. This is accompanied with an increase of the vortex strength and the forces acting on the wing.

4.4 Discussion

In the next section the tunnel wall corrections will be applied to the test data of the 76/40-deg double-delta wing. For these corrections the method developed by Garner and Rogers [6] was selected. Karou [13] has shown that this method gives good results for a 76-deg delta wing up to $\alpha = 22.5$ deg angle of attack. The improved correction for the averaged upflow parameter δ_0 suggested by Frink [7] will not be applied, because in order to be able to determine this parameter a FVS solution is needed for the flowfield over the double-delta wing. Such a solution is not provided in reference [7]. The wake blockage

correction proposed by Maskell [8] will not be applied either, because this correction can be determined only if the C_L^2 vs C_D curve is linear over a large range of angles of attack. Data computed in reference [1] indicate that this is not the case for a 76/40-deg double-delta wing (Fig. 15).

5 Corrections applied to BART Test Data

5.1 Blockage Effect

The ratio between the wing area and the cross-sectional area of the tunnel test section S/C is called the blockage ratio. For the present wing and tunnel, $S = 0.0711$ m^2 and $C = 0.724$ m^2, so that

$$S/C = 0.0982$$

Using the following data for the wing and tunnel,

$$\begin{aligned} B &= 1.02 \text{ m} \\ H &= 0.71 \text{ m} \\ V &= 2.015{*}10^{-3} \text{ m}^{3*} \\ \beta &\approx 1 \\ t &= 9.53 \text{ mm} \\ c &= 0.406 \text{ m} \end{aligned}$$

with equation 2 it can be calculated that

$$\epsilon_s = 0.00262$$

The solid blockage factor is independent of the angle of attack. This factor will also be affected by the post and sting which supports the wing in BART. In addition, the pressure tubes behind the wing (Fig. 3) may have some influence. Since the dimensions of these parts were not measured during the tests, the effect of these parts is not taken into account here for the solid blockage factor.

To compute the wake blockage factor with equation 4, a value is needed for the drag coefficient C_D. Because no balance measurements were conducted on the present wing, the force coefficients are used which were computed for the same wing by Kern [1]. He solved the flow over the wing in free air. An estimation is then needed of the effect of tunnel walls on C_L (and C_D). This has been obtained from data published by Washburn [14]. He compares balance data obtained for a 76-deg delta wing in the BART with data recorded with the same wing in the 7-ft by 10-ft tunnel at NASA LaRC. His data show an increase in C_L vs α due to tunnel wall interference. Another effect is that of the fairing at the lower surface of the wing. Washburn's data showed that the fairing only influences the effective wing camber but not the slope of the C_L vs α curve. The negative camber effect decreased the C_L by an average value of 0.04 throughout the angle of attack range. One of the differences between the flow over a 76-deg delta wing and that over a 76/40-deg double-delta wing is, e.g., that bursting occurs over the double-delta wing at already low angles of attack (Fig. 5). The burst location may be affected by the fairing on the lower surface of the wing. Guglieri and Quagliotti [15] studied the effect of a fairing at the lower surface of a 65-deg delta wing on the vortex breakdown location. At $\alpha = 20$ deg, the presence of the fairing resulted into a 20% chord more upstream location of the vortex burst.

In the following computations the effect of the tunnel wall interference and the fairing

*V = the estimated volume of the wing (.518*10^{-3} m^3) plus the estimated volume of the fairing (1.497*10^{-3} m^3)

on the C_L (and C_D) of the 76/40-deg double-delta wing is assumed to be the same as that measured by Washburn for the 76-deg delta wing in BART. The author is aware that this assumption is debatable and should be verified in future tests, if possible. The assumptions are made here since, to the author's knowledge, no other data is available to quantify these effects. Table 1 gives the values of C_D^1 computed in reference [1] for the wing in free air, of the estimated C_D for the wing in BART, and of ϵ_w for three angles of attack.

α (deg)	C_D^1 ref. [1]	C_D	ϵ_w eq. (4)
10	0.09	0.09	0.00221
15	0.21	0.22	0.00540
20	0.36	0.38	0.00993

Table 1.

To compute the streamwise-velocity interference factor with equation 5, the distance from the wing to the tunnel floor d should be known. This distance, unfortunately, was not measured during the testings at BART. Washburn [14] used the same support for a 76-deg delta wing and found that ([14], table B.1)

$$\frac{d}{H} = \frac{9.7" + 10.6" sin(19.8^o + \alpha)}{28"} \tag{10}$$

With this ratio

$$\delta(\frac{d}{H}, \frac{B}{H}) = \epsilon_v.(\frac{\beta BH}{S.C_L}) \tag{11}$$

can be determined using Fig. 3.3 of [6].

The computed values of C_L^1, C_L, $\frac{d}{H}$, δ and ϵ_v are given in table 2. C_L represents the estimated lift coefficient of the wing in BART.

α (deg)	C_L^1 ref. [1]	C_L	$\frac{d}{H}$ eq. (10)	δ eq. (11)	ϵ_v eq. (5)
10	0.34	0.35	0.535	0.018	0.00062
15	0.66	0.69	0.562	0.032	0.00216
20	0.86	0.90	0.589	0.046	0.00407

Table 2.

Summating the solid, wake and stream-interference factors yields the blockage factor ϵ_B. Substituting this factor into equation 6 gives the blockage correction for the dynamic pressure. Results are given in table 3.

α (deg)	ϵ_B eq. (1)	$\frac{q}{q_m}$ eq. (6)
10	0.00545	1.0190
15	0.01018	1.0204
20	0.01602	1.0320

Table 3.

Fig. 17 shows the variation of the different blockage factors with the angle of attack. The solid blockage is independent of α. It should by reminded that its value may be larger than calculated here due to the effect of the support and the pressure tubes. Both the wake and streamwise-velocity blockage can be seen to both increase with the angle of attack. The contribution of the wake blockage is the largest.

5.2 Lift Effect

The correction for the average velocity direction is computed using equation 7. According to reference [6], Fig. 3.2, for the present tunnel $\delta_0 = 0.116$ and $\delta_1 = 0.232$. No correction was applied for the off-center location of the wing. Fig. 3.3 of reference [6] suggests this correction to be small. The center of pressure x_p has been calculated using the computed force and moment data of again reference [1]. According to Washburn and Visser [16], the post support induced an upwash on the order of 2 deg. Table 4 gives the value of x_p, and the increase in effective angle of attack $\Delta\alpha$ due to the upwash computed with equation 7 and the upwash induced by the post support.

α (deg)	x_p (%c)	$\Delta\alpha$ (deg)
7.5	0.453	2.21
10	0.550	2.35
12.5	0.589	2.56
15	0.617	2.65
17.5	0.620	2.78
20	0.621	2.84

Table 4.

The increase in effective α leads to a larger vortex strength and lower upper-surface C_p. The C_p-distributions were corrected for $\Delta\alpha$ by linear interpolation between the data recorded at $\alpha+\Delta\alpha$-2.5 deg and $\alpha+\Delta\alpha$ deg.

5.3 Wall Corrections applied to C_p-Distributions

Figs. 18 and 19 show the effect of both the blockage and the lift effect correction on the C_p-distribution at 25 and 75% chord for $\alpha = 10$ and 20 deg, respectively. Applying the wall corrections, especially the lift correction, result into a much lower level of C_p and,

as shown in Fig. 20 for $\alpha = 10$, reduces the deficiency between the laminar solution and the experiment. Differences remain between the predicted and measured C_p-distributions, which can not fully be attributed to the small difference in Reynolds number used for the solution and the experiment. The differences are supposed to be due to inaccuracies in the wall interference correction procedure and the numerical modeling. It should further be reminded, that the corrections rely on wall effects measured by Washburn and Visser ([14] and [16]) on a 76-deg delta wing, and not a 76/40-deg double-delta wing, tested in the BART. It would have been interesting to compare the corrected data presented in Fig. 20 with the data measured on the 76/40-deg double-delta wing in the 7-ft by 10-ft tunnel at NASA LaRC. Unfortunately, the author of this report was not permitted to use the data measured in this tunnel.

6 Tunnel Wall Effects on Vortex Breakdown; A Literature Survey

The location of the vortex core breakdown over a delta wing is a function of the angle of attack, sideslip, roll angle, and leading-edge sweep. It is also affected by the geometry, beveling and thickness of the wing. Experimental data can be found in references [17] - [21], and others.
In this section the influence of the effect of tunnel walls on the vortex core breakdown location over a delta wing is discussed.

Weinberg [22] computed this effect using a method of vortex images. Inside the tunnel both leading-edge vortices and an additional pair of vortices representing the wing's bound vorticity were modeled. Along the wing an upwash distribution was calculated that was small near the apex and increased towards the trailing edge, indicating that an effectively cambered wing is created under the influence of the tunnel walls. Using a nonlinear vortex lattice method, he computed the distribution of C_p along the axis of the leading-edge vortex over a flat and a cambered delta wing. Above the flat wing C_p reached its lowest value at about 30% chord, while above the cambered wing the minimum C_p was located more downstream at about 50% chord due to the continuously increasing local α along the wing chord. Since breakdown is caused by an adverse pressure gradient, the vortices above the cambered wing can be expected to burst downstream of the breakdown location of the flat wing. Weinberg remarks that this conclusion is opposite to the intuition that wall effects tend to increase the effective α. Such an increase would result in correcting the breakdown location towards the trailing edge, whereas the appropriate correction, when taking the effective camber into account, is towards the apex. Weinberg investigated the wall effect in a water tunnel experiment using two sets of three delta wings which had a leading-edge sweep angle of 60 and 70 deg. The three wings in each set increased linearly in size, while keeping a similar wing geometry. For the 70-deg wings, the breakdown location was observed to move continuously downstream as the wing increases in size. This is in accordance with the predicted trend. The breakdown location for the 60-deg wings did not follow the predicted trend as well as the wings with the higher sweepback. Weinberg concluded that his method of images is valid for small aspect ratio wings only.

Pelletier and Nelson [23] investigated the effect of tunnel walls on three 70-deg swept delta wings that also increased linearly in size and were geometrically similar. The tests were conducted in a water tunnel at Re = 35,000 and angles of attack up to 45 deg. The results showed that for a given α the vortex breakdown location moved upstream with increasing wing size, and hence increasing blockage. This does not agree with the abovementioned test results of Weinberg and his theory of effective camber. Pelletier and Nelson modeled the tunnel walls using four image vortices (two for each leading-edge vortex). The image vortices induce an upwash which increases with wing size and leads to a larger effective α. According to their theory, the location of the vortex breakdown on a larger wing should thus be upstream of that on a smaller wing because the wing experiences a larger α. This is in accordance with the observations in their water tunnel experiment. They further showed that the vortex breakdown location of the three wings

tend to match when the change in velocity at the model due to blockage is taken into account.

7 Conclusions and Recommendations

Surface-pressure data of a 76/40-deg double-delta wing tested in the BART at NASA LaRC were corrected for tunnel wall interference effects using a flowfield correction method. The correction is shown to improve the correlation between the computed and measured C_p-data. Deficiences between the computed and measured C_p remain and may be due to inaccuracies in the wall correction procedure and the numerical modeling.

To improve the accuracy of experimental dataset, it is recommended to include balance measurements in future wind tunnel tests and to pay attention to the effect of the wing support and the fairing at the lower surface of the wing on the balance data.
It is further recommended to include the tunnel walls and support configuration in the numerical model.

Surprisingly few experimental data is available on the effect of tunnel walls on the location of vortex core breakdown. Published data of experiments in water tunnels show contradictory results. To obtain a better insight and more unique information on the effect of the tunnel walls on vortex breakdown, it is recommended to study this effect by conducting tests in water and wind tunnels with (double-)delta wings of different size. NAWC has an excellent wind tunnel at PAX River to carry out this type of testings. The testings in a water tunnel could be performed using the facility of the Naval Post Graduate School at Monterey. Besides these experiments, solutions of the Navier-Stokes equations could also help obtain a better understanding of this wall effect.

8 Acknowledgements

The author wishes to acknowledge Mark Maurice of EOARD for his directions and support to obtain the current Special Contract. Acknowledge is also given to Steven Kern and Hugo Gonzalez of NAWC for the useful discussions and the interesting visits to their research facilities.

9 References

References

[1] Kern, S.B., "Numerical Investigation of Vortex Flow Control Through Small Geometry Modifications at the Strake/Wing Junction of a Cropped Double-Delta Wing," AIAA-92-0411, Reno, January 1992

[2] Verhaagen, N.G., Jenkins, L.N., Kern, S.B. and Washburn, A.E., "A Study of the Vortex Flow over a 76/40-deg Double-Delta Wing," AIAA-95-0650, Reno, Januari 1995, and ICASE Contractor Report 95-5, February, 1995

[3] Sellers III, W.L. and Kjelgaard, S.O., "The Basic Aerodynamics Research Tunnel," AIAA-88-1997, San Diego, May 1988

[4] Visser, K.D. and Washburn, A.E., "Transition Behavior on Flat Plate Delta Wings," AIAA-94-1850, Colorado Springs, June 1994

[5] Hummel, D., "Zur Umstroemung scharfkantiger schlanker Deltafluegel bei grossen Anstellwinkeln," ZFW 15, 1967, Vol. 10, pp. 376-385

[6] Garner, H.C. and Rogers, E.W.E., "Subsonic Wind Tunnel Wall Corrections," AGARDograph 109, 1966

[7] Frink, N.T., "Computational Study of Wind-Tunnel Wall Effects on Flow Field around Delta Wings," AIAA 87-2420, 1987

[8] Maskell, E.C., "A Theory of the Blockage Effects on Bluff Bodies and Stalled Wings in a Closed Wind Tunnel," A.R.C. R.&M. 3400, Nov. 1963

[9] Pass, C.Q., "A Wake Blockage Correction Method for Small Subsonic Wind Tunnels," AIAA-87-0294, Reno, Jan. 1987

[10] Hackett, J.E., Wilsden, D.J. and Stevens, W.A., "A Review of the Wall Pressure Signature and Other Tunnel Constraint Correction Methods for High Angle-of-Attack Tests," AGARD-R-692, Feb. 1981

[11] Thomas, J.P. and Lan, C.E., "The Simulation and Correction of Wind Tunnel Wall Interference on Delta Wing Lift using Navier-Stokes and Euler Solutions," AIAA-91-3300-CP, Baltimore, Sept. 1991

[12] Verhaagen, N.G., Houtman, E.M. and Verhelst, J.M., "A Study of Wall Effect on the Flow over a Delta Wing," AIAA-96-2389, New Orleans, June 1996

[13] Karou, A., "Separated Vortex Flow over Slender Wings between Side Walls," TUDelft Report LR-300, August 1980

[14] Washburn, A.E., "The Effect of Freestream Turbulence on the Vortical Flow over a Delta Wing," MSc Thesis, Rolla, December 1990

[15] Guglieri, G. and Quagliotti, F.B., "Experimental Investigation of Vortex Dynamics on a 65-deg Delta Wing," AIAA Paper 92-2731-CP, June 1992

[16] Washburn, A.E. and Visser, K.D., "Evolution of Vortical Structures in the Shear Layer of Delta Wings," AIAA-94-2317, June 1994

[17] Lambourne, N.C. and Bryer, D.W., "The Bursting of Leading-Edge Vortices - Some Observations and Discussion of the Phenomenon," A.R.C. R&M No. 3282, Great Britain, April 1961

[18] Wentz, W.H. and Kohlman, D.L., "Vortex Breakdown on Slender Sharp Edged Wings," *Journal of Aircraft*, Vol. 8, No. 3, 1971, pp. 156-161

[19] Payne, F.M., Ng, T.T. and Nelson, R.C., "Experimental Study of the Velocity Field on a Delta Wing," AIAA-87-1231, 1987

[20] Kegelman, J. and Roos, F., "Effects of Leading-Edge Shape and Vortex Burst on the Flowfield of a 70 Degree Sweep Delta-Wing," AIAA-89-0086, Reno, Jan 1989

[21] Straka, W.A. and Hemsch, M.J., "Effect of a Fuselage on Delta Wing Vortex Breakdown," *Journal of Aircraft*, Vol. 31, No. 4, 1994, pp. 1002-1005

[22] Weinberg, Zvi, "Effect of Tunnel Walls on Vortex Breakdown Location over Delta Wings," *AIAA Journal*, Vol. 30, No. 6, June 1992

[23] Pelletier, A. and Nelson, R.C., "Factors Influencing Vortex Breakdown over 70-deg Delta Wings," AIAA-95-3469-CP, 1995

10 Figures

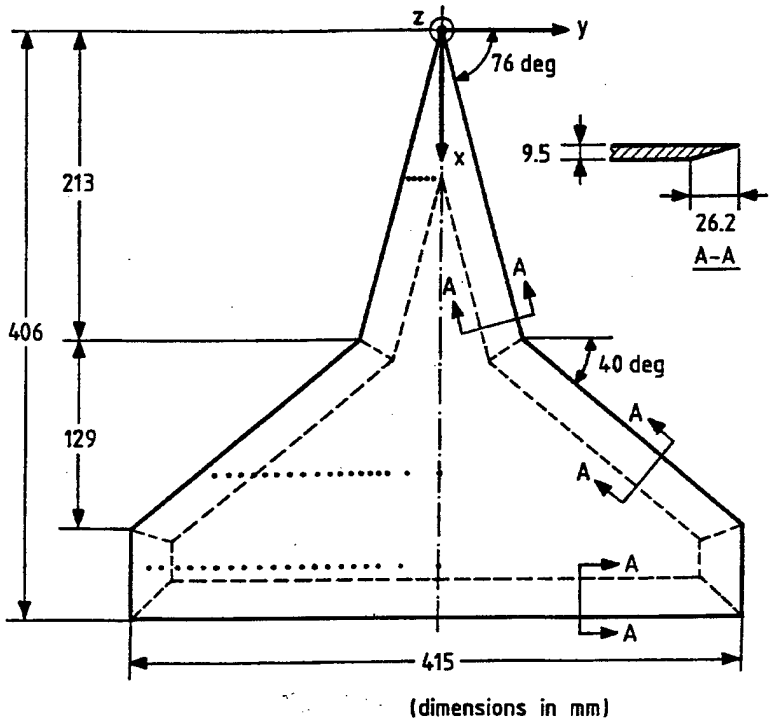

Figure 1: Double-delta wing geometry

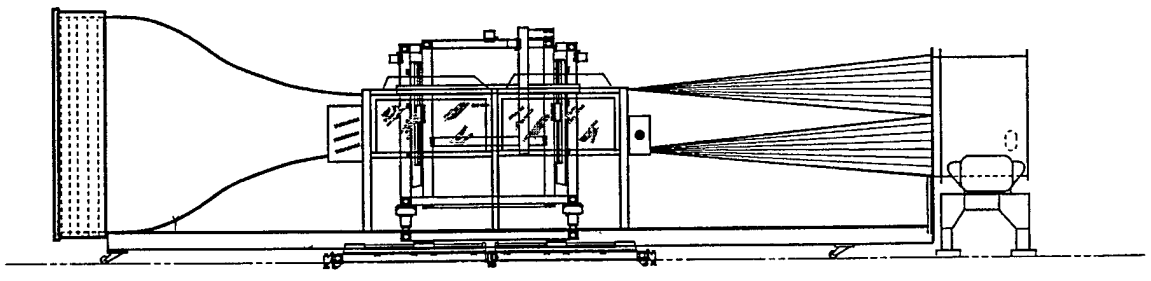

Figure 2: BART tunnel

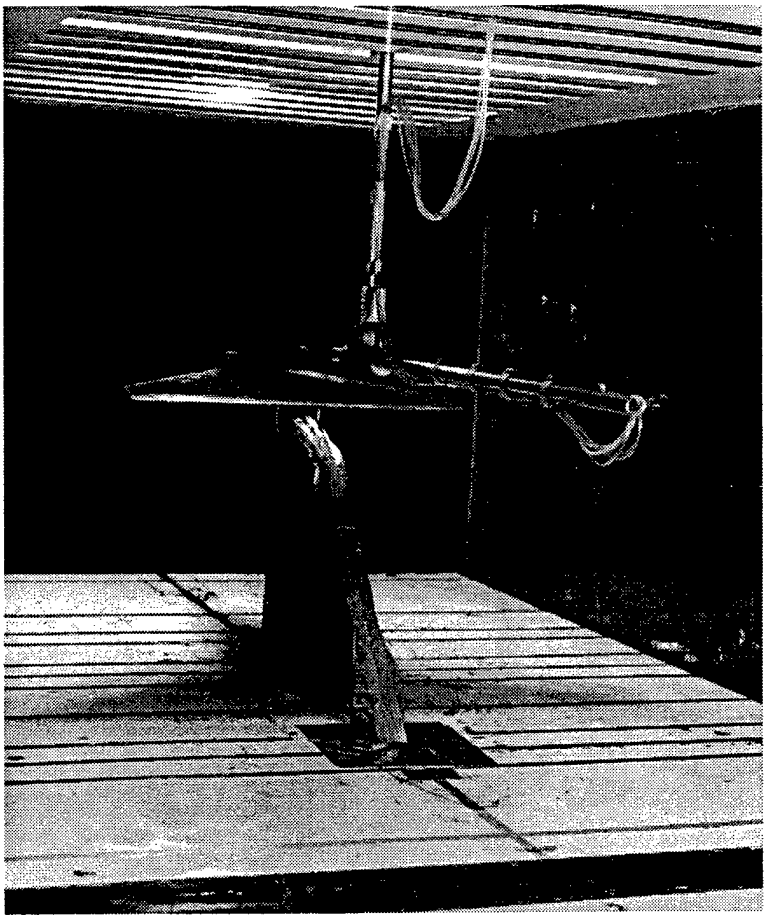

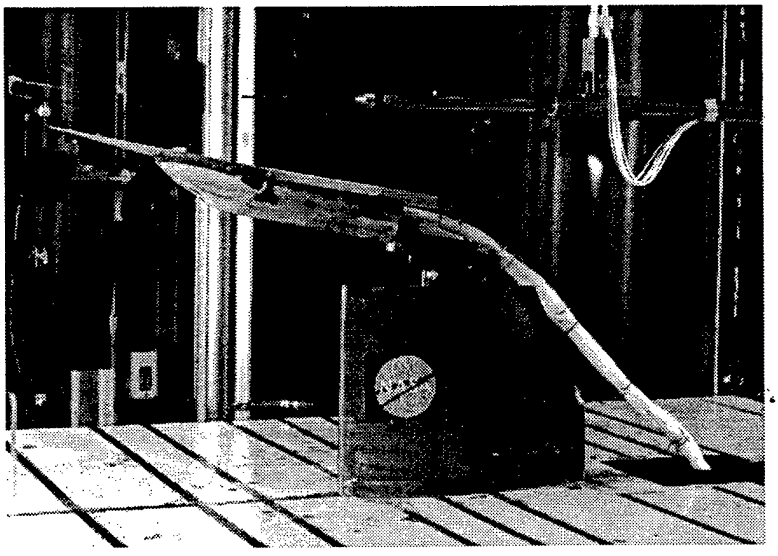

Figure 3: Wing in BART tunnel

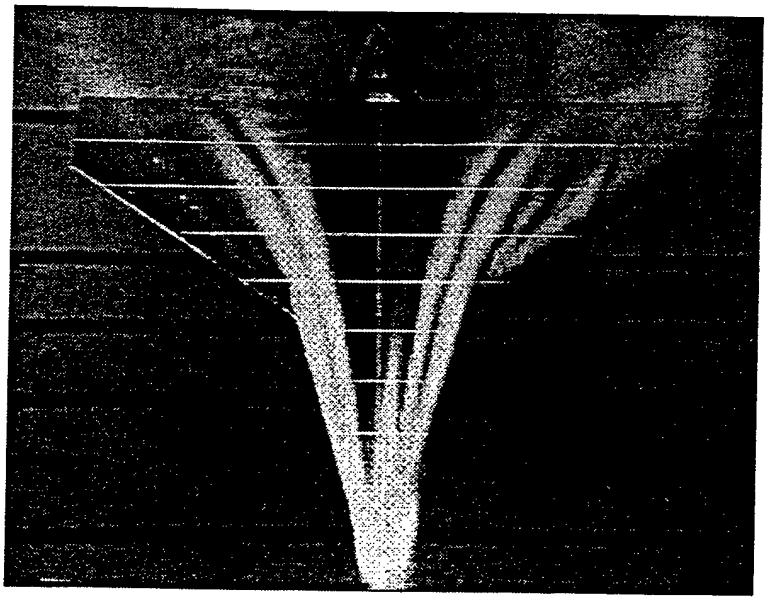

Figure 4: Vortices illuminated by laserlight sheet; $\alpha = 10$ deg

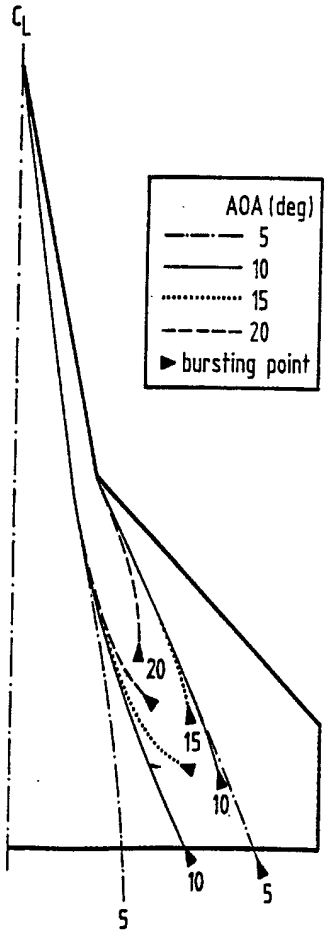

Figure 5: Effect of α on vortex axis trajectory and core burst location

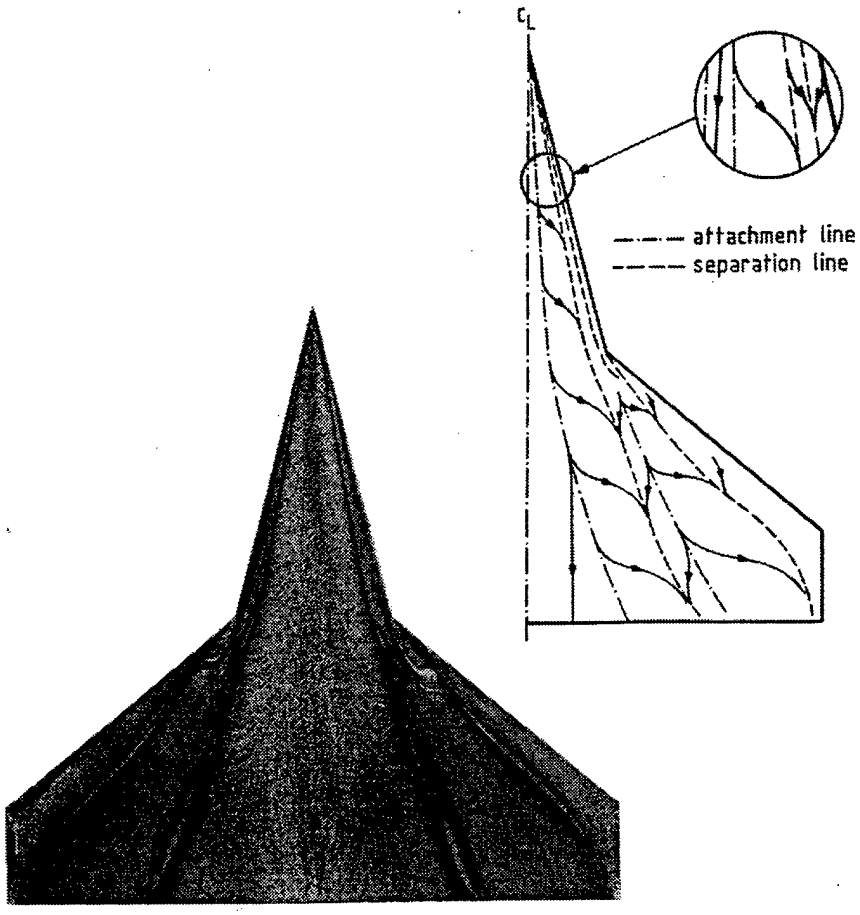

Figure 6: Upper surface flow pattern; $\alpha = 10$ deg, $Re = 1.0$ M

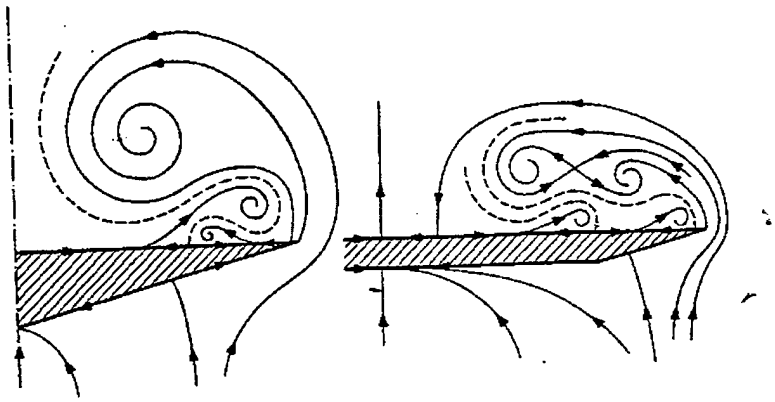

Figure 7: Topology of crossflow over strake (left) and wing (right sketch)

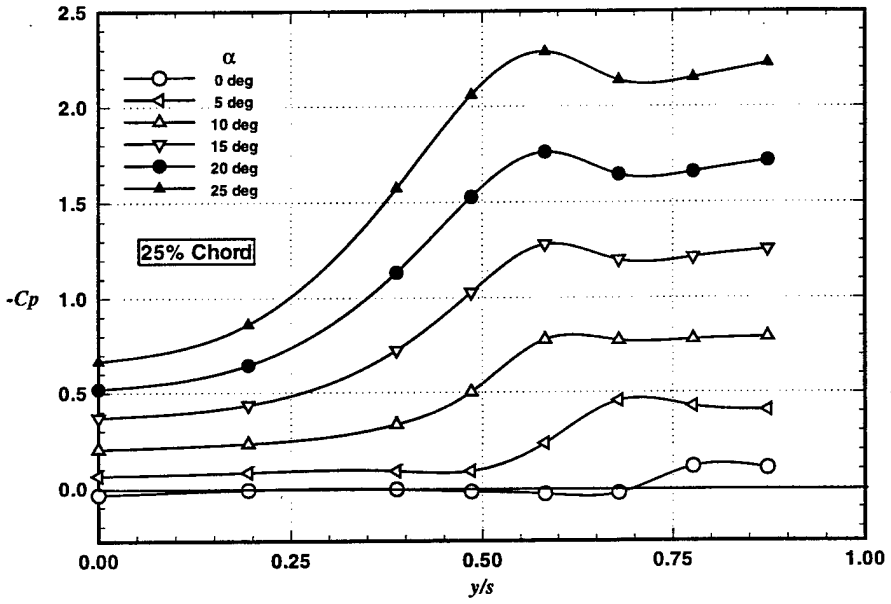

Figure 8: Effect of α on upper-surface C_p at 25% chord; $Re = 1.0$ M

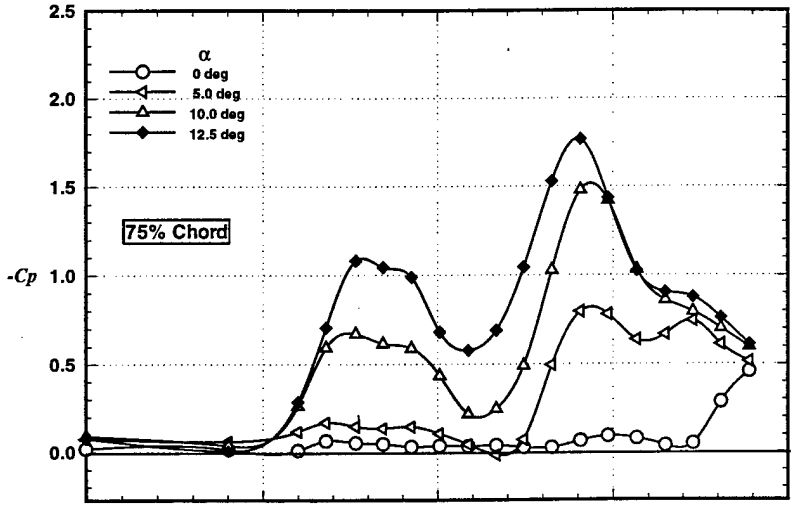
α
0 deg
5.0 deg
10.0 deg
12.5 deg
75% Chord
-Cp
2.5
2.0
1.5
1.0
0.5
0.0

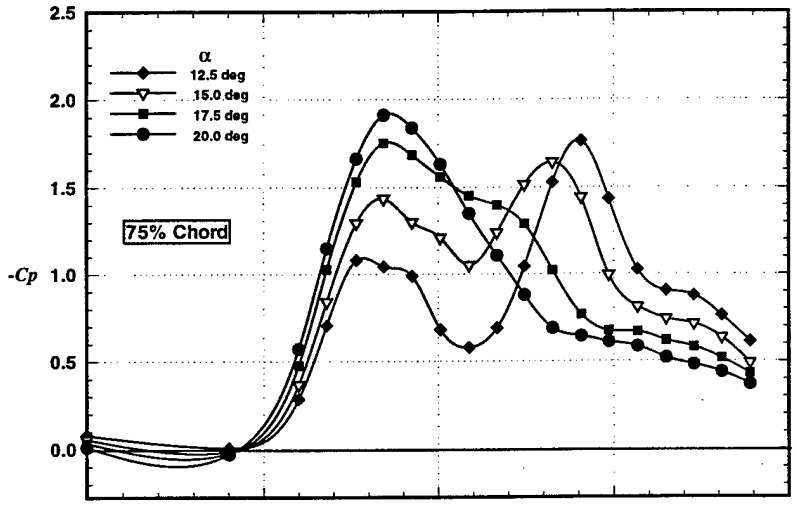
α
12.5 deg
15.0 deg
17.5 deg
20.0 deg
75% Chord
-Cp
2.5
2.0
1.5
1.0
0.5
0.0

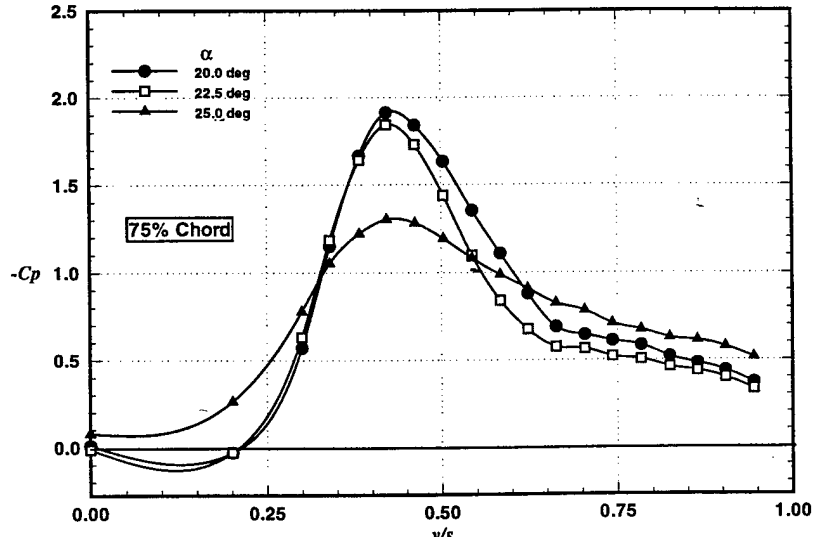
α
20.0 deg
22.5 deg
25.0 deg
75% Chord
-Cp
2.5
2.0
1.5
1.0
0.5
0.0
0.00
0.25
0.50
0.75
1.00
y/s

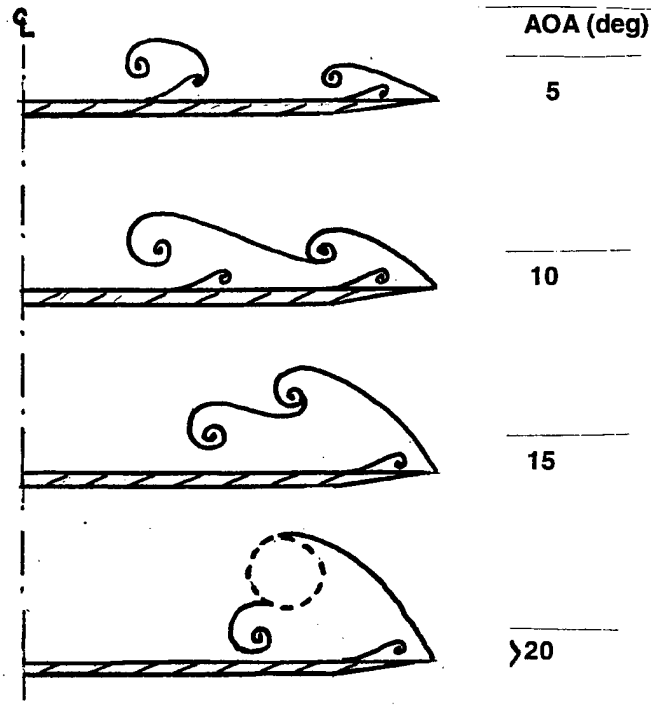

Figure 10: Effect of α on crossflow topology at 75% chord

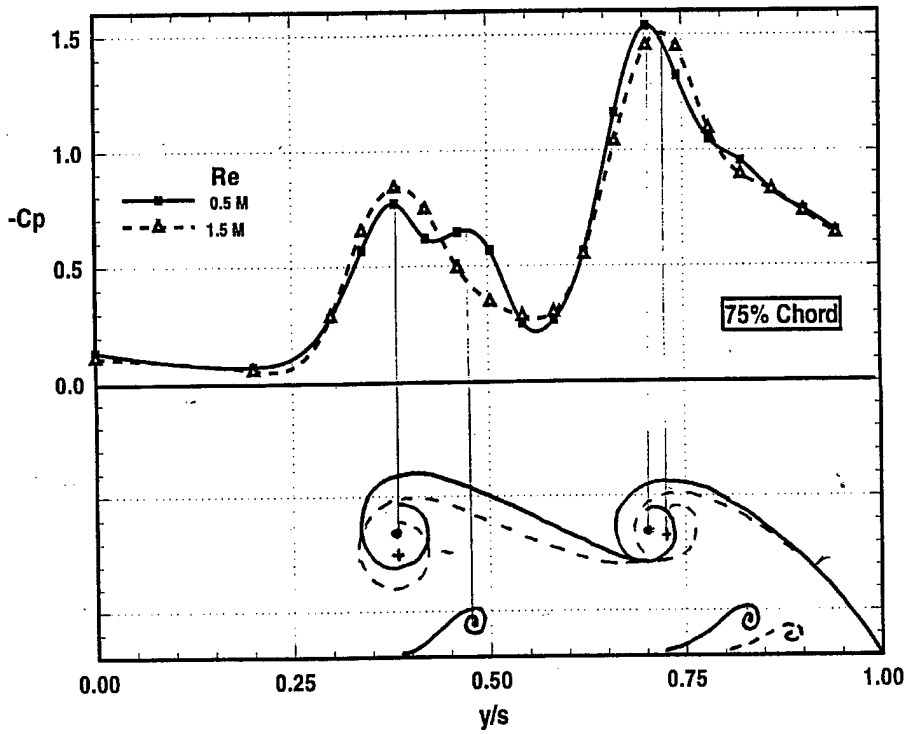

Figure 11: Effect of Re on upper-surface C_p at 75% chord; $\alpha = 10$ deg

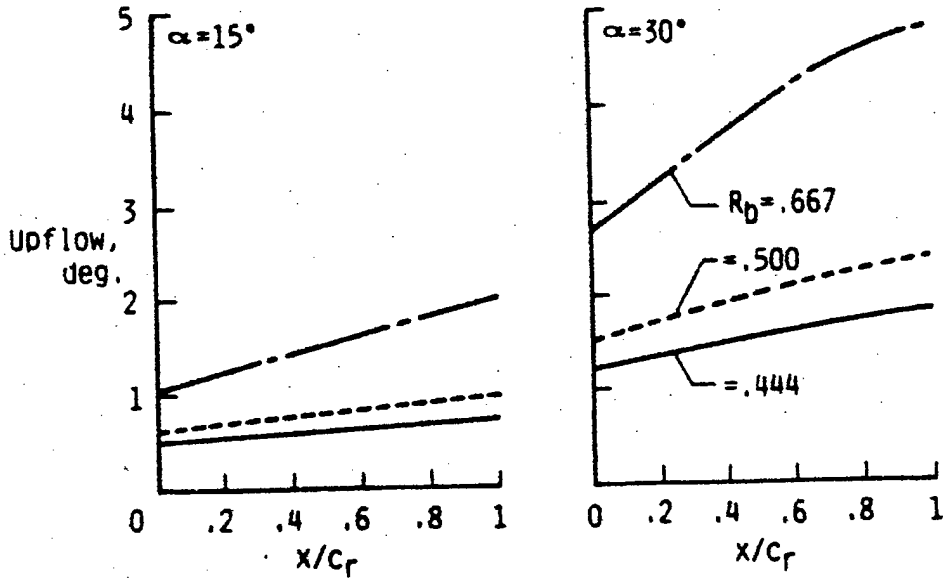

Figure 12: Computed effect of R_b on streamline curvature along root chord; 65 deg delta wing, $R_t = 2.5$ (Frink [7])

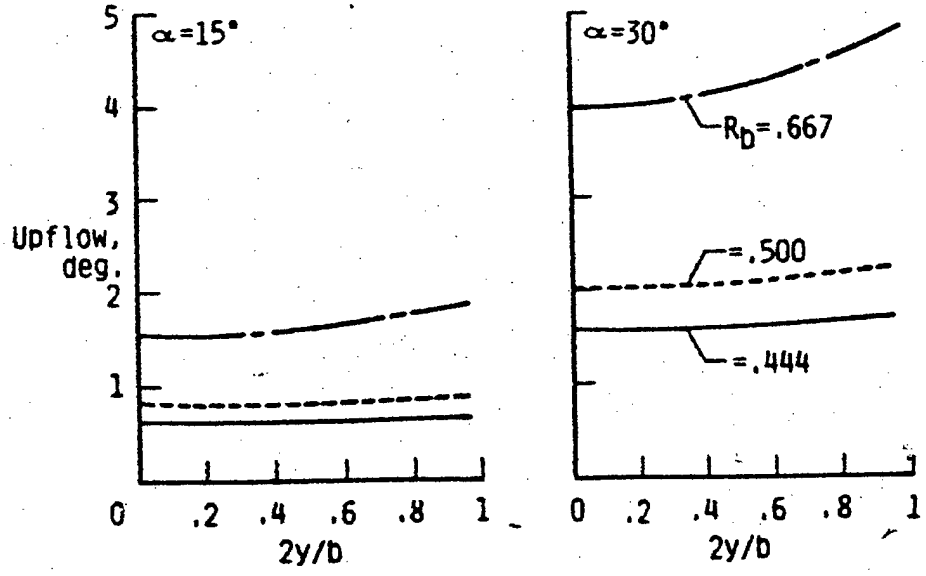

Figure 13: Computed effect of R_b on aerodynamic twist at mid chord station; 65 deg delta wing, $R_t = 2.5$ (Frink [7])

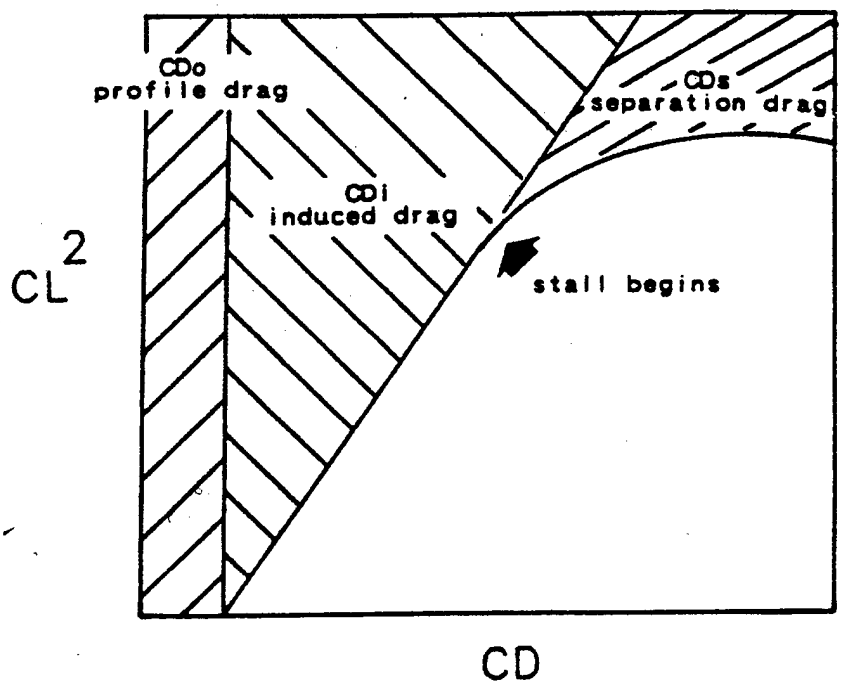

Figure 14: Method of separating drag components (Maskell [8])

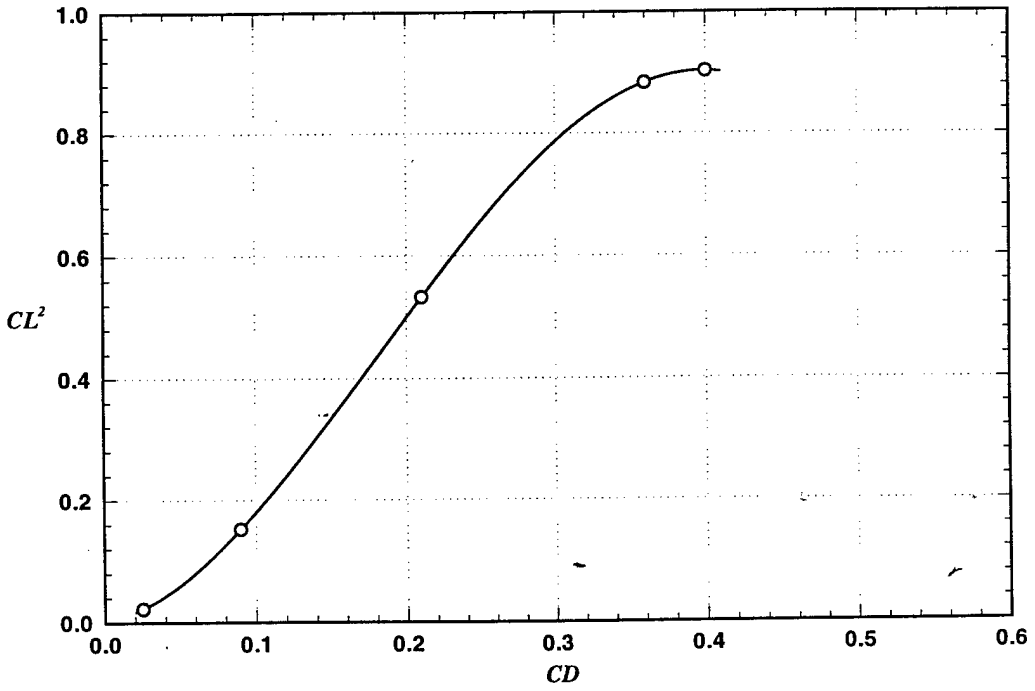

Figure 15: Computed C_L^2 vs C_D (Kern [1])

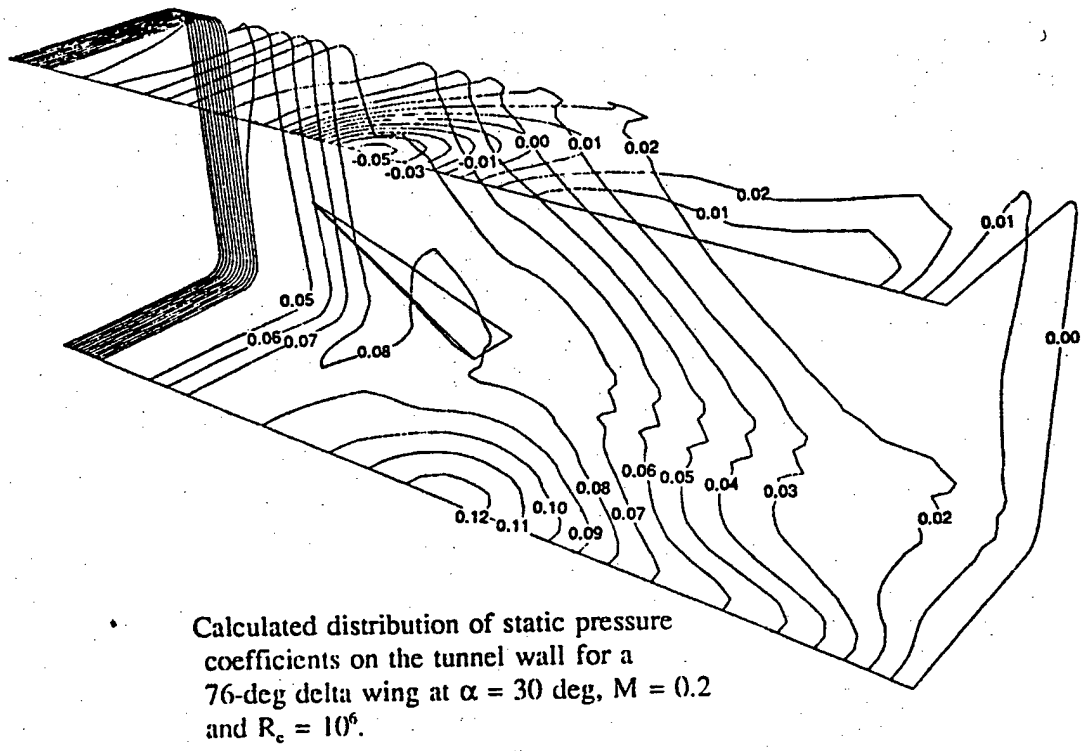

Figure 16: Computed C_p-distribution induced on walls of BART by a 76-deg delta wing (Thomas and Lan [11])

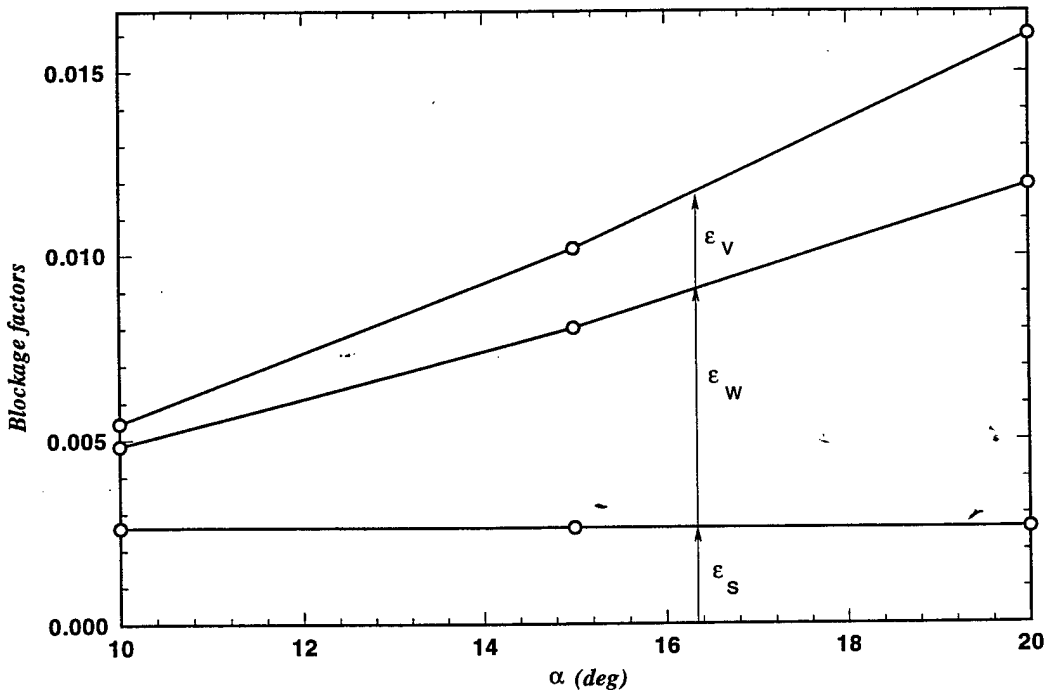

Figure 17: Effect of α on blockage correction factors

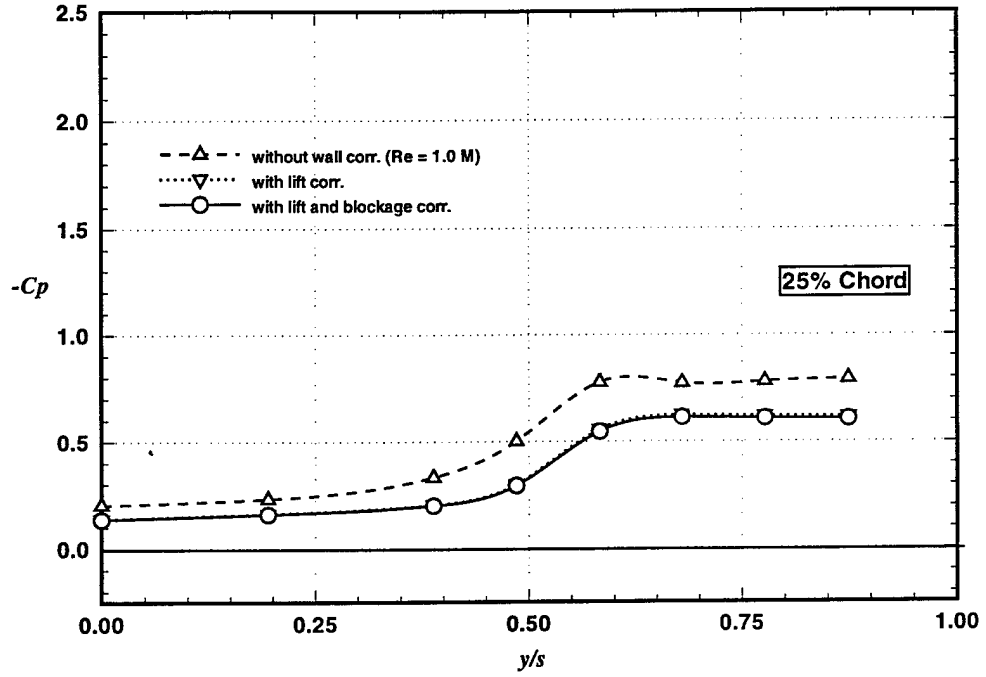

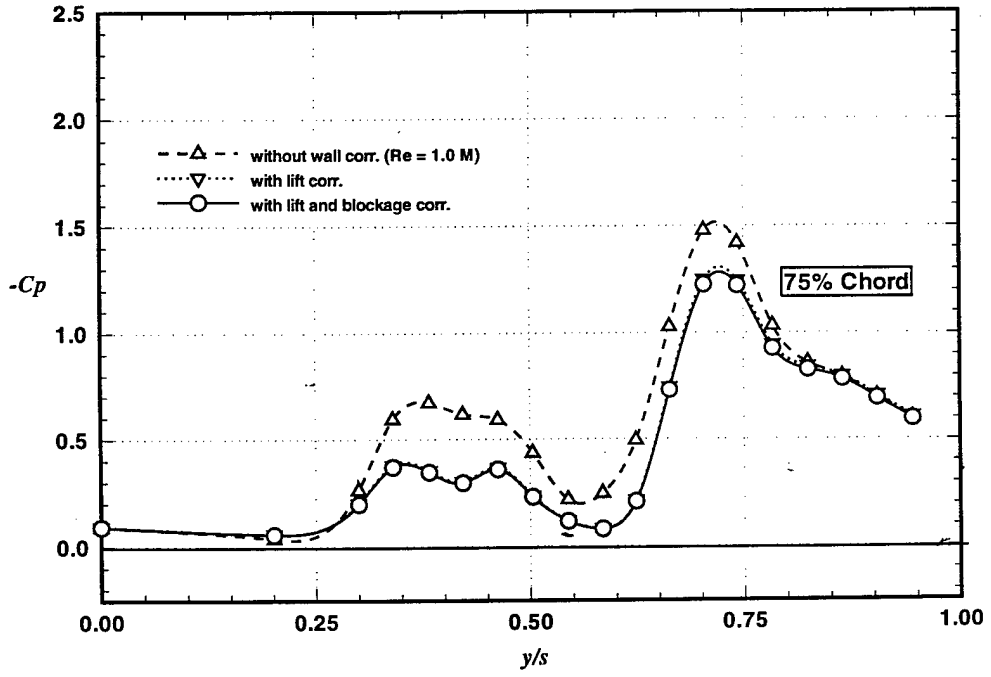

Figure 18: Effect of lift and blockage corrections; $\alpha = 10$ deg, $Re = 1.0$ M

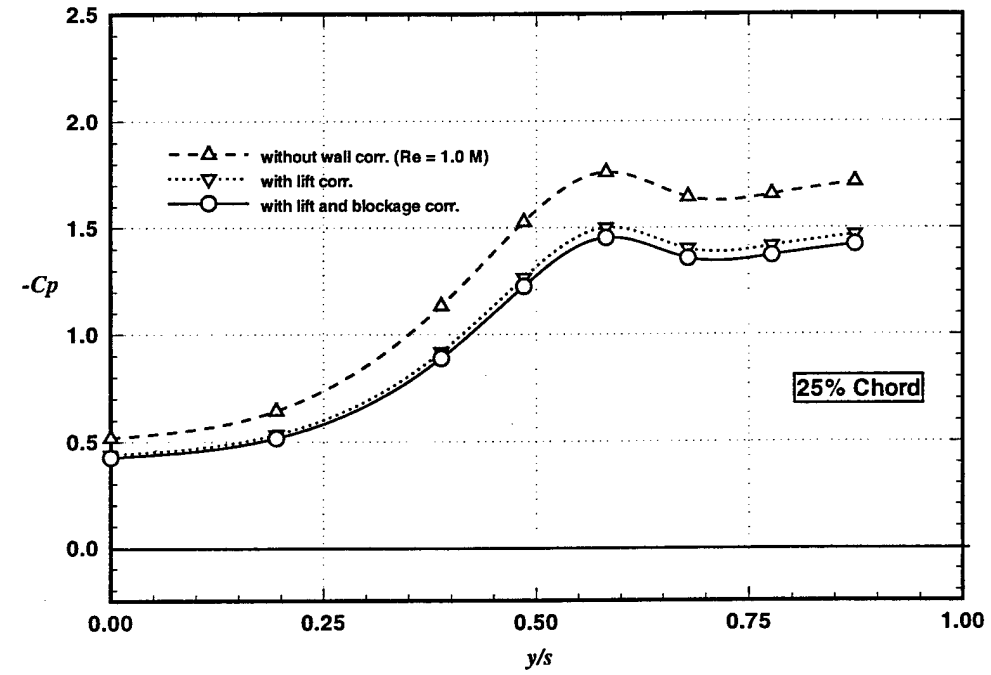

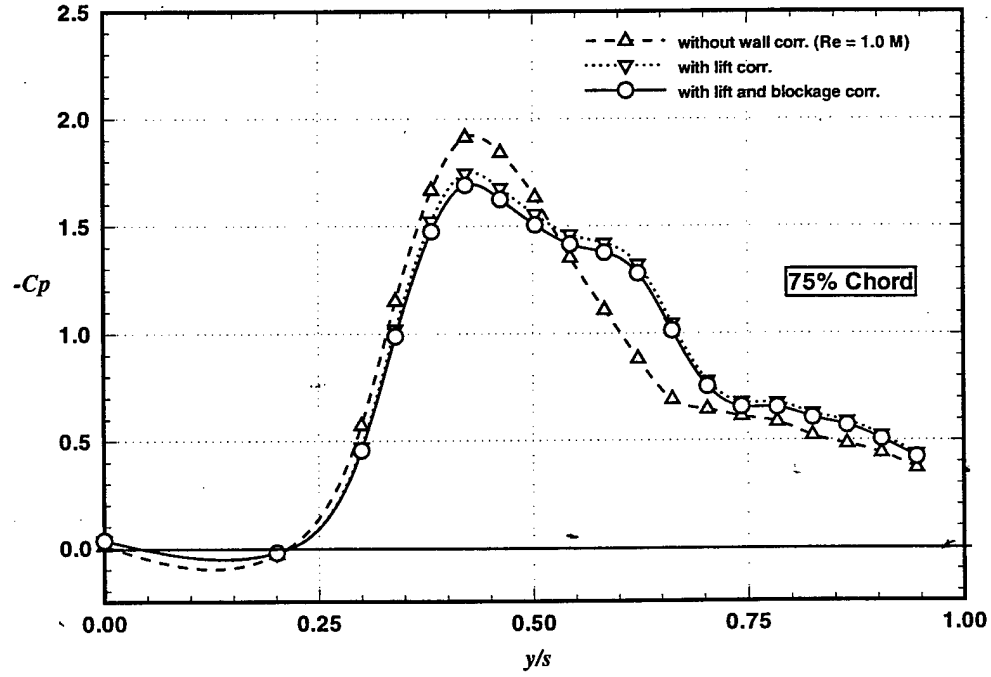

Figure 19: Effect of lift and blockage corrections; $\alpha = 20$ deg, $Re = 1.0$ M

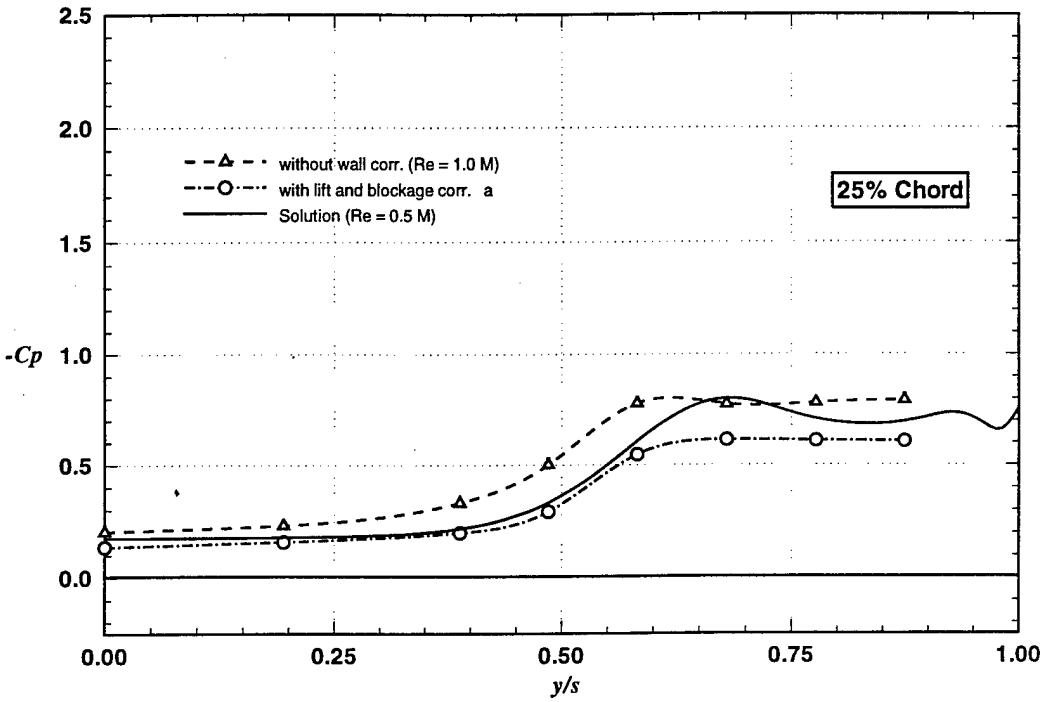

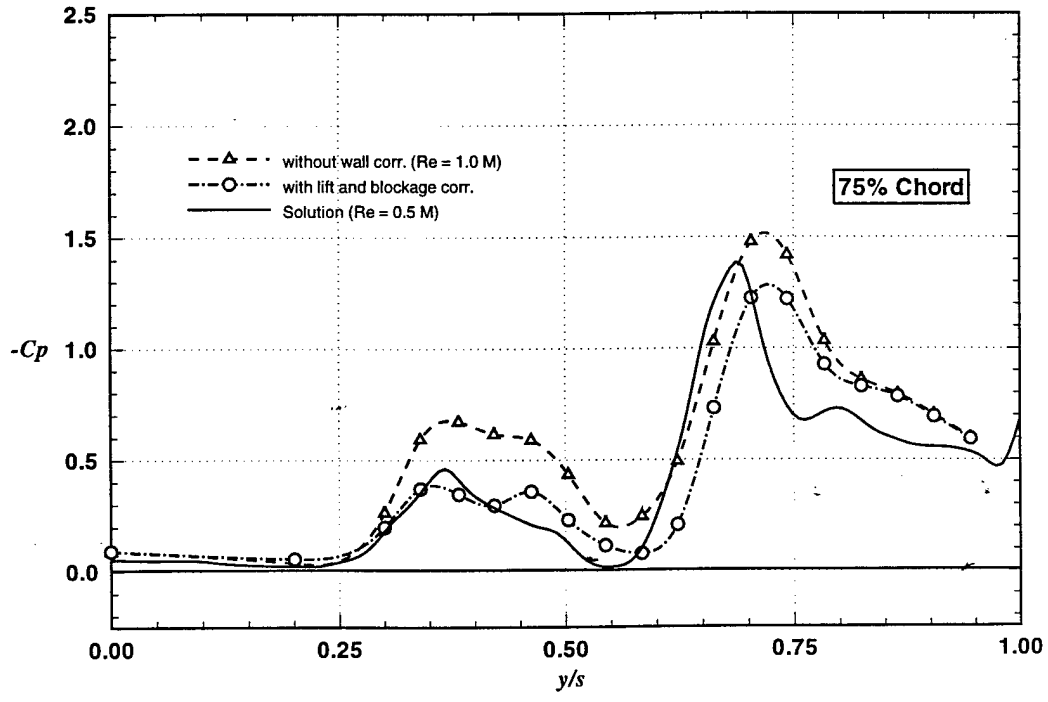

Figure 20: Comparison between solution and experiment; $\alpha = 10$ deg